Connective-Tissue Fibroblasts Established on Micropillar Interfaces are Pivotal for Epithelial-Tissue Morphogenesis**

By *Eva Mussig, Thorsten Steinberg,* *Simon Schulz, Joachim P. Spatz, Jens Ulmer, Niels Grabe, Annette Kohl, Gerda Komposch,* and *Pascal Tomakidi*

This work is dedicated to Professor Norbert Fusenig in appreciation of his excellent leadership as head of the "Department of Differentiation and Carcinogenesis" of the German Cancer Research Center

Polydimethylsiloxane (PDMS) pillar arrays are applied as a biomechanical microenvironment to establish gingival connective-tissue fibroblasts (GCTFs) and to further analyze the pivotal role of GCTFs in epithelial-tissue morphogenesis. GCTFs are known to exert successful adhesion and growth on fibronectin immobilized on pillar heads, over time, concomitant with the increased gene expression of vimentin and collagen type-I. GCTF-populated pillar arrays clearly reveal that epithelial-tissue morphogenesis of immortalized human gingival keratinocytes (IHGKs), co-cultured for 7 and 14 days, parallels the in vivo phenotype more closely, when compared with GCTF-free control arrays. This in vivo-like phenotype is substantiated by higher mRNA levels for keratin 1, involucrin and filaggrin differentiation markers. Furthermore, it is reflected by a tissue-specific protein orientation of the aforementioned molecules, and also of the cell-to-cell contact forming desmoplakin and the basement membrane constituents, laminin-5, laminin-1/10, and collagen type-IV. These experiments suggest that the in vivo-like phenotype of the IHGK is governed by the GCTFs growing on the micropillar interfaces. Moreover, they form the basis for the optimization or neogeneration of biomaterials by varying predefined microenvironmetal parameters to achieve an in vivo-like cell growth and differentiation, indispensable for tissue morphogenesis during regeneration.

[*] Dr. T. Steinberg, Dr. E. Mussig, A. Kohl, Prof. G. Komposch
Prof. P. Tomakidi
Department of Orthodontics and Dentofacial Orthopaedics,
University of Heidelberg
Im Neuenheimer Feld 400, 69120 Heidelberg (Germany)
E-mail: thorsten.steinberg@med.uni-heidelberg.de

S. Schulz, Prof. J. P. Spatz
Department of Biophysical Chemistry, University of Heidelberg
Im Neuenheimer Feld 253, 69120 Heidelberg (Germany)

S. Schulz, Prof. J. P. Spatz, Dr. J. Ulmer
Max Planck Institute for Metals Research
Heisenbergstr. 3, D-70569 Stuttgart (Germany)

Dr. N. Grabe
Department of Medical Informatics, University of Heidelberg
Im Neuenheimer Feld 400, 69120 Heidelberg (Germany)

Dr. N. Grabe
Hamamatsu TIGA Center, BIOQUANT, University of Heidelberg
Im Neuenheimer Feld 267, 69120 Heidelberg (Germany)

1. Introduction

Combining material technologies with life sciences will be the prerequisite for optimizing already-existing biomaterials or even creating new materials for the use in regenerative medicine. To achieve this goal, it will be of fundamental importance to study the multiple interactions of cells of certain tissues with their microenvironment. Understanding the microenvironment and the deduction of defined microenvironmental parameters in particular will be the key to learning tissue-innate requirements, which in turn will lead to proper cell growth and tissue morphogenesis. Hereby, the cells form tissue themselves or assist in the morphogenesis of an adjacent tissue by providing pivotal interdependencies, which also exist in vivo. In this context, biomechanics, which describes the interplay of mechanical forces between the extracellular environment and a distinct cell type, appears to be an important parameter. To detect the traction forces that cells or biomolecules exert on their underlying substrates, micro-arrays of elastic pillars or posts which are biofunctionalized with extracellular-matrix constituents, such as fibronectin (FN) for cell adhesion are currently widely used.[1–5] In addition, flat or planar flexible substrates are also suitable tools to calculate forces exerted by cells on their microenvironment.[6–10] In distinction to elastic pillars, planar elastomeric surfaces are

more easily fabricated. However, one major disadvantage of the latter substrates emerges from their limited resolution in traction-force microscopy, which is described by the elastic Green functions,[11] and results from the surface thickness.[7] This disadvantage requires complex mathematical calculations to invert the system of coupled integral equations given by linear elasticity theory, which relate the substrate deformation to the force.[12] Despite the mentioned drawbacks, such kinds of substrate are popular, since they circumvent the complex photolithography indispensable for the construction of the elastomeric micropillar surfaces. Considering the previously mentioned disadvantages of planar elastic substrates, we have chosen pillar surfaces which have the advantage that no complex calculations are necessary to obtain the forces, as each pillar behaves like an elastic spring: the deflection is proportional to the force.[6] Concerning the above-mentioned interdependencies between cells of two tissues, the present study demonstrates for the first time that the connective-tissue fibroblasts established on FN-coated pillar microarrays are pivotal for epithelial morphogenesis. This inclusion of keratinocytes as a second cell type extends the current applicability of pillars as tools for cell traction-force sensors by showing that fibroblasts growing in a defined biomechanical environment are capable of directing in trans the formation of an epithelial tissue.

In vivo, the interdependencies of fibroblasts located in the epithelium-underlying connective tissue (CT) with keratinocytes are indispensable for the maintenance of the epithelial-tissue homeostasis.[13] This homeostasis which is characterized by its cornerstone, the balance of proliferation and differentiation, is orchestrated by the complex interplay of diffusible molecules, also known as growth factors.[14] Due to loco regional differences, the CT of skin epithelium is termed *dermis*, while that of the oral cavity gingival epithelium is termed *lamina propria*.[15] Contrasting its corresponding epithelium, the CT is poorly populated by cells, while it mainly consists of extracellular-matrix (ECM) molecules including various collagens, FN and a variety of proteoglycans.[16] These CT matrix components which, as a base substance, constitute the cells' microenvironment are synthesized by the cells themselves prior to secretion. Thus, CT fibroblasts produce multiple collagens, among which collagen type-I is the most abundant matrix molecule in the CT. Moreover, fibroblasts can be characterized by their intermediate filament (IF) vimentin, a feature that they share with other cells of mesenchymal origin. The CT-epithelial junction zone is defined by a group of highly organized ECM molecules forming the basement membrane (BM). BM constituents are collagen type-IV, laminin-1/10, and laminin-5.[17] Squamous epithelia of skin and oral-cavity gingiva consist of several cell layers reflecting progressive stages of epithelial cell differentiation. Proliferation of epithelial cells, that is, keratinocytes, which are detectable by reliable proliferation markers, occurs in the basal cell layers proximal to the BM, while early and terminal differentiation are restricted to suprabasal and apical epithelial layers. Biomarkers of early keratinocyte differentiation are keratins (K) K1 and K10, belonging to the family of IF proteins, while terminal differentiation is specified through involucrin and filaggrin.[18,19] Additional markers, such as desmoplakin, indicate the presence of cell-to-cell contacts, thereby featuring epithelial integrity. In total, the latter-described molecules are hallmarks of epithelial homeostasis. Therefore, we have used them as biomarkers to monitor epithelial-tissue morphogenesis in response to GCTFs established on FN-coated PDMS pillar microarrays.

In contrast to our approach of investigating epithelial morphogenesis of keratinocytes based on fibroblasts established in a defined traction-force-sensing microenvironment, previous morphogenetic studies employed connective-tissue cells incorporated in a collagen lattice.[20–22] Studies with an emphasis on biomechanics described lattice contraction by oral or dermal connective-tissue cells or in response to fibroblasts to various growth factors,[23] but usually gave no approximation of the fibroblast-exerted traction forces. In a recently published paper, modeling of a spongy collagen lattice using the Euler column buckling model yielded contractile forces of dermal fibroblasts in a range from 10–41 nN. Unlike our strategy, this study was based on a nonconfigured microenvironment.[24]

Here, we performed studies on epithelial morphogenesis by using fibroblasts grown on FN-coated pillars holding a defined biomechanical elasticity module (Young's modulus) of 2.5 MPa. In this context, our interest was of dual nature. Firstly, it was focused on the cell adhesion of GCTFs on pillar model surfaces, combined with the calculation of traction forces and, conversely, whether the calculated forces facilitate the cells' ability to propagate and synthesize specific biomolecules. Secondly, we were interested in the role of GCTFs growing in such a defined microenvironment on the epithelial morphogenesis of immortalized human gingival keratinocytes (IHGKs). From the biological point of view, it should be noted that in addition to morphological changes, epithelial morphogenesis is reflected by the expression and distinct topography of certain biomarkers that are genetically determined through the keratinocyte differentiation program. Among others, we therefore analyzed biomarkers assigned to early and terminal differentiation at both the mRNA and protein level.

In regenerative medicine and dentistry in particular, strategies based on tissue engineering and modification of biomaterials with biomolecules seem to be promising tools for the management of lost periodontal tissues. In tissue engineering, in addition to stem cells and signaling molecules, scaffolds of extracellular-matrix molecules comprising collagen, fibrin, hydroxyapatite or FN amount to hopeful strategies to support the healing process.[25] In addition, FN was also used as a biomodifier of titanium-based dental implants in animal in vivo and in vitro studies employing cell cultures.[26,27] Thus, covering the pillar heads with FN makes the defined PDMS-microarrays used in our study more bioconvenient for cells. In total, such conditions are suitable for studying cell adhesion and growth and for determining cell-derived traction forces. These conditions for this part will form

the basis for optimization or neogeneration of biomaterials by varying predefined environmental parameters to achieve an in vivo-like cell growth and differentiation, indispensable for tissue morphogenesis during regeneration.

2. Results and Discussion

2.1. The Establishment of GCTFs on Micropillar Interfaces Allows Measurement of the Traction Forces and Analysis of the Growth Behavior

One key to designing a defined microsensing microenvironment for the GCTFs is to create PDMS pillar microarrays with defined height, distance and diameter. This has been achieved using molds with a defined height and diameter and photolithography preceding emulsification of the molds with a photoreactive polymer.[25] In our studies, the pillars were arranged with a head diameter of 5 μm, a height of 15 μm, and an interspace of 9 μm. To allow for discrete cell adhesion and calculation of traction forces, only the pillar heads were biofunctionalized with FN.[4] Using the above-described defined microenvironment, we first attempted to establish GCTFs by seeding 7.8×10^3 cells per cm^2. Figure 1A shows the adhesion of single and confluent GCTFs on the FN-coated pillar heads, 24 h after seeding, by phase-contrast microscopy and raster electron microscopy (REM), as demonstrated in the corresponding inset. In the high-power magnification of the red-marked cell (Fig. 1A), three pillars are highlighted by red rings (Fig. 1B); two of them are used as non-deflected controls to calculate the cell's traction force, while the deflected pillar indicated by the larger red circle clearly reveals successful cell adhesion on the FN-biofunctionalized pillar heads (Fig. 1C, deflected pillar). For small deflections, the pillars behave like simple springs such that the deflection is directly proportional to the force applied by the attached cell. This behavior, for beams composed of linearly elastic material under pure bending, is described by the force-deflection relationship in Equation (1):[29]

$$F = k \cdot \Delta x = \frac{3}{4}\pi E \frac{r^4}{L^3} \cdot \Delta x \qquad (1)$$

In Equation (1), k is given by standard linear elastic beam theory, r, L and Δx are the

radius, length and deflection of the pillar and E is the Young's modulus.

Symbols representing deflected and non-deflected pillars have been used to generate the traction-force diagram for GCTFs (Fig. 1D). Herein, the oscillation of the magenta graph reflects the direction of the GCTF-induced pillar deflection, indicating a maximum traction force of approximately 174 nN per pillar, when calculating the vector sum of the force directions. Since
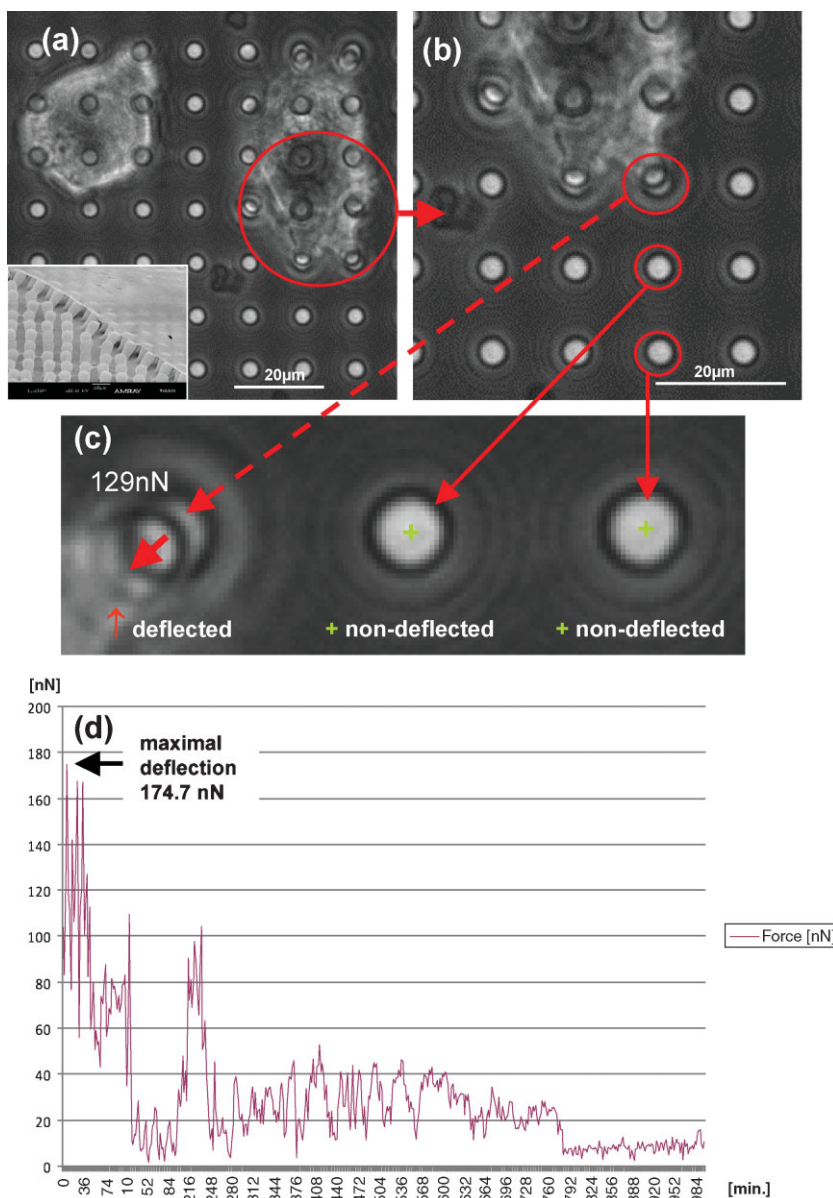

Figure 1. A) Live-cell imaging using phase-contrast microscopy displays a single GCTF (red circle) on an FN-coated micropillar array with 9 μm pillar interspaces. The inset illustrates a REM picture depicting a confluent GCTF sheet on the pillar heads. B) Detailed enlargement of A) showing deflection (larger red circle) of a single pillar resulting from adherent GCTF traction forces, while non-deflected (red rings) pillars serve as fixed points for traction-force calculation. C) A snapshot from a live-cell-imaging movie, where the traction force can be calculated as 129 nN at this time point, considering the plotted marks of non-deflected (+) and deflected (↑) pillars. D) Determination of traction forces exerted by a single GCTF on a single pillar over time (∼16 h) with a maximal deflection of 174.7 nN. The bars in parts A and B correspond to 20 μm.

we were further interested in the growth behavior of the cells, GCTF-populated pillar microarrays derived from co-cultures with IHGKs were monitored at day 7 and 14, after careful removal of the epithelial compartment. REM revealed that the cells had reached a subconfluent density at day 7 (Fig. 2A1), while they were nearly confluent at day 14 (Fig. 2B1). These differences in density were corroborated by indirect immunofluorescence (IIF), demarcating more cells as positive for the connective-tissue cell-specific vimentin (Fig. 2(A–B)) and collagen type-I (Fig. 2 (C–D)) molecules at the later culture period (Fig. 2B and Fig. 2D).

Interestingly, real-time polymerase chain reaction (RT-PCR) of these molecules demonstrates that the pillars on which the GCTFs have grown close to confluence exhibit approximately seven-fold levels of mRNA transcription for both genes, when compared to the subconfluent pillar arrays (Fig. 2E, compare day 7 and 14). These results strongly suggest that GCTFs can be successfully established in the chosen defined microenvironment, and that they are obviously capable of proliferating on the pillar microarrays when co-cultured with IHGKs. This assumption is supported by the REM-inset in Figure 1A which shows that the fibroblasts can form a confluent tissue sheet on the biofunctionalized pillar heads when grown for periods extending 14 days. In this context it appears noteworthy that the higher cell densities observed at the later time point of 14 days coincide with an increased biosynthesis of molecules that characterize the connective tissue fibroblasts. Thus, the chosen regime may be considered as suitable to form a gingival connective-tissue equivalent under defined biomechanical in vitro conditions, and appears versatile to study the modulation of tissue-innate morphogenesis or morphogenesis of an epithelial tissue in trans by prospectively varying certain microenvironmental parameters in terms of pillar biomechanics or pillar biofunctionalization. Conversely, the traction forces calculated above (see Fig. 1D) reflect a GCTF innate force range that is obviously favorable for the observed biological behavior described in our study.
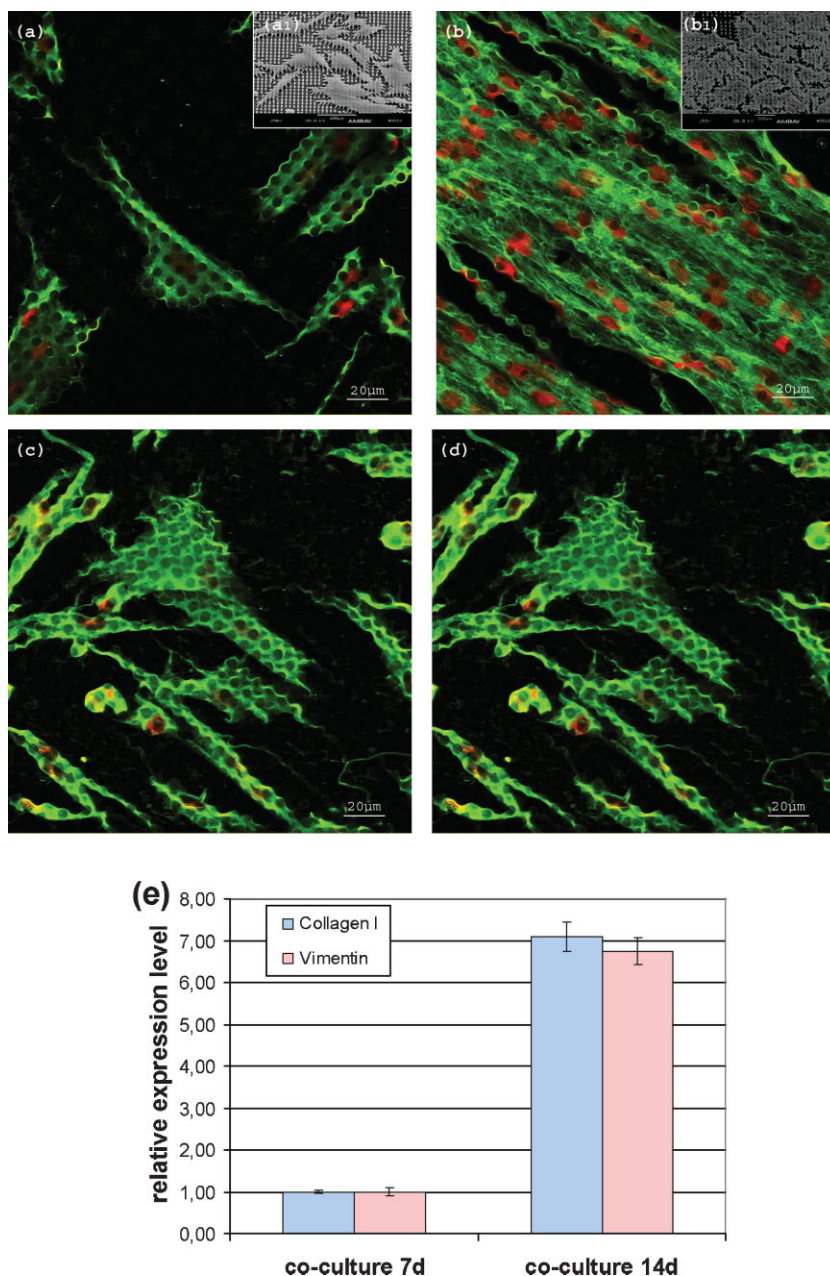

Figure 2. Microscopy techniques illustrate the growth behavior of GCTFs derived from co-cultures with IHGKs on FN-coated micropillar surfaces. A1) REM depicts the subconfluence of GCTFs after a 7 day culture period, while B1) reveals a nearly confluent density after 14 days. IIF demarcates an increased number of vimentin/collagen type-I positive cells after 14 days (B,D) culture period, compared with the situation after 7 days (A,C). Red propidium iodide (PI) counterstain demarcates the cell nuclei. E) Quantitative real-time PCR displays markedly increased gene-expression level for connective-tissue cell-specific vimentin (pink columns) and collagen type-I (blue columns) molecules at the later culture period of 14 days, compared with 7 days. The relative expression levels were analyzed using a modification of the $\Delta\Delta C_T$ equation, which allows for differences in efficiencies ($E = 10^{-1/slope}$) between the PCR reactions. [21] The data were calculated using the Gene Expression Macro software provided with the iCycler. The data were normalized to the C_T of the glycerinaldehyd-3-phosphat-Dehydrogenase (GAPDH) non-modulated housekeeping gene. The data reflect the means ($n = 3, \pm SD$) of three independent experiments. The bars correspond to 100 μm (A1, B1) and 20 μm (A–D).

2.2. The Impact of GCTFs Established on Micropillar Interfaces on Epithelial Morphogenesis

To explicitly study the role of GCTFs established on biofunctionalized micropillar interfaces on epithelial morphogenesis of IHGKs, we generated co-cultures of these two cell types and matched controls only comprising the keratinocytes. The mode of operation of the co-culture technique together with the corresponding control is illustrated in Figure 3.

To mimic the in vivo situation which is characterized by spatially separated growth of connective-tissue fibroblasts and keratinocytes, we used a collagen type-I cell-culture matrix in case of *posterior* conduction of IIF in the epithelial compartment (Fig. 3A), and the trans-well system in order to isolate selectively the RNA from both cell types, devoid of cell-type cross contamination (Fig. 3B). Irrespective of the respective co-culture system, the GCTFs were established on the pillar microarrays as previously described and precultured for 24 h before being overlaid with the collagen lattice or the trans-well filter insert. Following the preculture period, IHGKs were seeded on the collagen lattice surface or on the porous membrane of the filter insert at a density of 1.0×10^5 cm^2, and co-cultured for 7 and 14 days. Empirically, these two time points are known from our previous co-culture studies using

conventional non-defined collagen type-I microenvironments to successively yield satisfactory epithelial morphogenesis. This satisfactory epithelial morphogenesis is essentially based on two features provided by the co-culture device using collagen lattices. Firstly, both cell types grow in a spatially separated manner. Secondly, due to this spatial separation, the interactions between the epithelial keratinocytes and the connective-tissue fibroblasts resemble that under in vivo conditions.[20–22] In the case of controls with keratinocytes only, they were handled as described above, but the pillar microarrays were devoid of fibroblasts (Fig. 3C and 3C1). The putative trans-active role of the pillar-standing GCTFs for epithelial morphogenesis has been initially evaluated in a comparative analysis between co-cultures and controls by quantification of gene expression and detection of the protein orientation of the biomarkers typical for early and terminal differentiation in squamous epithelia. For this purpose, the epithelial compartments of co-cultures and controls, either derived from the collagen lattice or the trans-well mode, were prepared for IIF or RNA extraction, respectively.

Concerning co-cultures, normalization to the GAPDH housekeeping gene revealed fairly constant levels of relative gene expression of the early differentiation marker, K10, at both time points (Fig. 4A), while for K1 a 7.39-fold drastic increase was detected at day 14 relative to day 7 (Fig. 4A). With respect to the markers indicating terminal differentiation, comparison of the culture periods under study displayed a slight elevation of 1.78-fold for involucrin at day 14 (Fig. 4C), while filaggrin showed a clear increase of 6.16-fold at the later time point (Fig. 4C). At day 7, the controls where the IHGKs were solely cultured on the collagen type-I lattice surface or optionally on the filter insert's porous membrane paralleled the relative gene expression levels found in co-cultures for these genes (Fig. 4B: K1 and K10; Fig. 4D: involucrin and filaggrin). Except for K10, the later culture period of 14 days revealed clear discrepancies for the other genes between IHGKs derived from co-cultures and controls. K10 transcription (Fig. 4B) appeared similar to co-cultures at both time points (Fig. 4A), but also to the controls at 7 days (Fig. 4B). In marked contrast, mRNA quantities detected for K1 (Fig. 4B), involucrin and filaggrin (Fig. 4D) were notably inferior in the controls when compared to the contemporaneous co-cultures (Fig. 4A and Fig. 4C). Inside the controls, the K1 and involucrin transcription was lower at day 14 in relation to day 7 (compare Fig. 4B, and 4D), while filaggrin showed almost equal levels at both culture periods (Fig. 4D).

The calculated transcript quantities clearly demonstrate drastic differences for genes related to early and terminal keratinocyte differentiation between the IHGKs of controls and co-cultures, which appeared most pronounced for K1 and filaggrin. Based on this comparative experimental setup these results strongly suggest that relative gene expression noted for K1 and filaggrin in the IHGKs is directly dependent on the in vivo-like tissue interactions provided by the GCTFs, established and growing on the defined FN-biofunctionalized pillar array microenvironment.
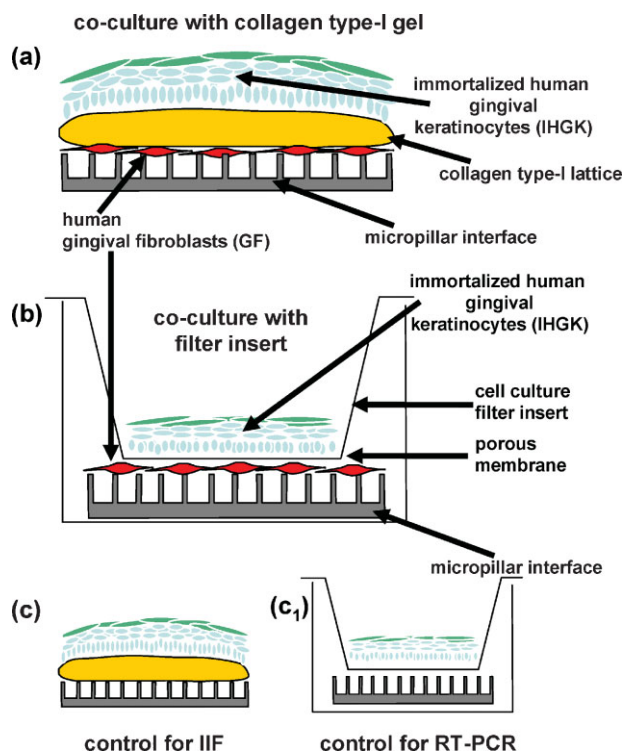

Figure 3. Schematic overview showing the mode of operation of the co-culture system and the respective controls. A) Co-culture mode used for indirect immunofluorescence (IIF) experiments. B) Co-culture mode applied for quantitative real-time-PCR (RT-PCR) experiments using the trans-well culture system. C and C1) Control mode for IIF and RT-PCR experiments lacking GCTFs.
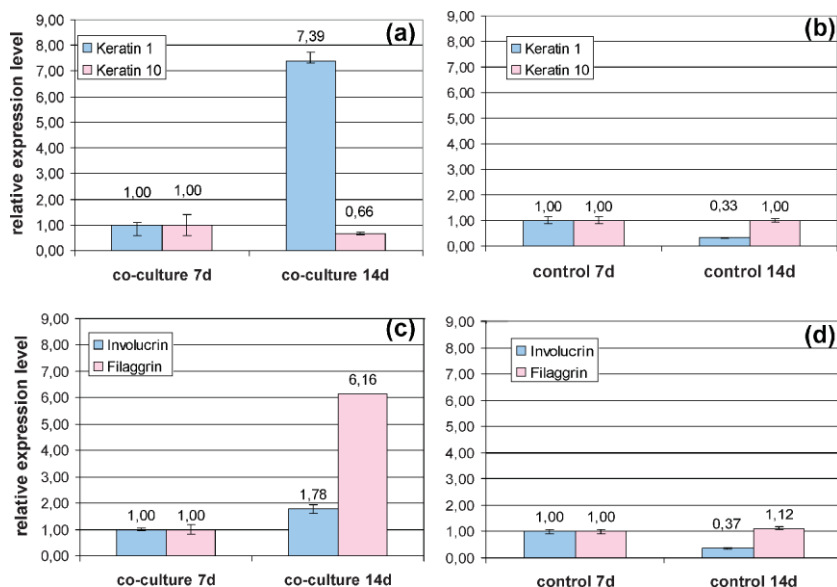
Figure 4. Quantitative real-time-PCR from immortalized human gingival keratinocytes (IHGKs) derived from the co-culture trans-well system, cultivated for 7 and 14 days, and matched controls. RT-PCR indicates the relative expression level of the Keratin (K) 1 (blue columns), and K10 (pink columns) early differentiation markers derived from the IHGK co-cultures (A), and the respective controls (B). RT-PCR shows the expression level of the involucrin (blue columns) and filaggrin (pink columns) late differentiation markers derived from the IHGK co-cultures (C), and the respective controls (D). The relative expression levels were analyzed using a modification of the $\Delta\Delta C_T$ equation, which allows for differences in efficiencies ($E = 10^{-1/\text{slope}}$) between the PCR reactions. [39] The data were calculated using the Gene Expression Macro software provided with the iCycler. The data were normalized to the C_T of the glycerinaldehyd-3-phosphat-dehydrogenase (GAPDH) non-modulated housekeeping gene. The data reflect the means ($n = 3, \pm$ SD) of three independent experiments.

2.3. Spatial Biomarker Orientation in Epithelial Equivalents Obtained from Co-cultures and Controls as Detected by IIF

We were interested in monitoring the orientation of the biomarkers previously analyzed on the transcriptional level: therefore, IIF was performed on frozen sections of epithelial compartments grown on collagen lattices at corresponding time points. At day 7, the expression of the keratin K1 and K10 early differentiation markers was inhomogeneous in the epithelial equivalents of the co-cultures (Fig. 5A). Concerning the terminal differentiation markers, involucrin was clearly present and mostly apparent in the uppermost cell layers (Fig. 5C), while filaggrin displayed a diffuse expression (Fig. 5E). The co-cultures at day 14 showed a clear and homogenous expression for K1 and K10, which, to some extent, already started in the basal cell layer (Fig. 5B), while involucrin was distinctively seen in the whole suprabasal epithelial compartment (Fig. 5D), and filaggrin appeared largely restricted to the apical cell layers (Fig. 5F). Exhibiting the protein orientations just described, the epithelial equivalents formed by the IHGKs at day 14 in the presence of GCTFs, previously established on the micropillar interfaces, resemble the in vivo phenotype of the oral gingival epithelium fairly well.[30,31] By comparison, the matched controls (Fig. 5(A–F), insets) were largely devoid

of K1/10 at day 7 (Fig. 5A, inset), which also applied for filaggrin (Fig. 5E, inset), while involucrin (Figure 5C, inset) was patchily expressed in the apical epithelial layers. Excluding involucrin (Fig. 5D, inset), which showed an homogenous suprabasal distribution, K1/10 (Fig. 5B, inset) and filaggrin (Fig. 5F, inset) if detectable at all appeared irregularly expressed at the later culture period.

Although not analyzed by light microscopy, propidium iodide red fluorescence used for total nuclear counterstain in IIF reveals that the IHGKs have the propensity to form epithelial equivalents comprising fewer cell layers when grown on GCTF-free pillar arrays (compare insets with the corresponding images in Fig. 5). This observation suggests that the fibroblasts support keratinocyte growth and differentiation in the co-culture situation, thereby yielding a more in vivo-like phenotype.

This hypothesis is backed up by considering two markers that indicate epithelial proliferation and integrity (Fig. 6). IIF detection of the *Ki*-67 antigen which renders a reliable proliferation marker[32] revealed fewer *Ki*-67-labeled cells in the IHGK co-cultures at day 14 (Fig. 6B) when compared with day 7 (Fig. 6A). On the other hand, no label was found in the controls at both time points (data not shown).

The lower *Ki*-67-label in the IHGK co-cultures may be a hint that the growth, that is to say the proliferation, declines over time concomitant with a gain of epithelial differentiation, as indicated by the status of the analyzed biomarkers. Studies on murine desmoplakin (DP) knockout keratinocytes have proven this molecule to be indispensable for epithelial integrity, since it supports reinforcement of membrane attachments essential for stable intercellular adhesion during cell-layer formation.[33] Since DP is clearly detectable in the IHGK co-cultures at both time points (Fig. 6C, day 7; and Fig. 6D, day 14), but not in the controls at day 7 (Fig. 6C, inset), and only scattered at day 14 (Fig. 6D, inset), it can be speculated that the epithelial integrity is less distinctive in the controls, a feature which may also be reflected by the reduced formation of cell layers in conjunction with the less in vivo-like orientation of the studied biomarkers of differentiation.

In addition to differentiation, proliferation, and integrity, a further hallmark of epithelia is the synthesis of specialized ECM molecules, which are essential constituents of the BM underlying all epithelia. Therefore, we further explored whether the GCTFs growing on the heads of the defined pillar microarrays are a pivotal component for orchestrating the in trans site-specific expression of BM-constituting ECM
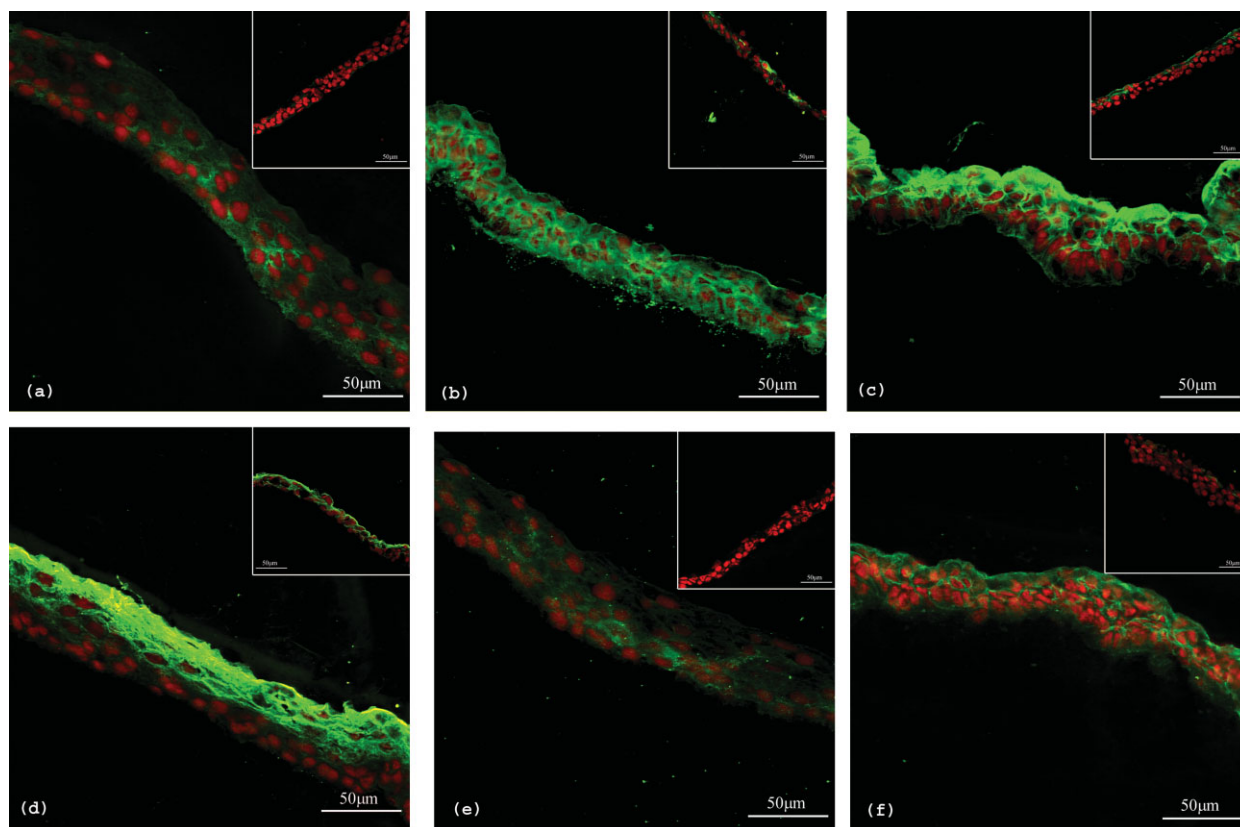
Figure 5. Indirect immunofluorescence illustrates the early and late differentiation markers, K1/10, involucrin and filaggrin, in co-cultured epithelial equivalents generated on micropillar interfaces after 7 and 14 days, and their matched controls. A) After 7 days, expression of the keratin K1/10 early differentiation markers was inhomogeneous, while at day 14 expression for K1 and K10 showed a clear and homogenous distribution that, to some extent, already started in the basal cell layer (B). At day 7, the involucrin terminal differentiation marker was clearly seen and mostly apparent in the uppermost cell layers (C), while filaggrin displayed diffuse expression (E). At the later time point, involucrin was distinctively seen in the suprabasal epithelial compartment (D), and filaggrin appeared to be largely restricted to the apical cell layers (F). The matched controls (A–F, insets) were largely devoid of a specific fluorescence signal or revealed irregular and patchy protein orientation at the later time point. The red propidium iodide (PI) counterstain demarcates the cell nuclei. The scale bars correspond to 50 μm.

molecules including laminin-5, laminin-1/10, and collagen type-IV in the epithelial equivalents. Regarding the above-mentioned set of molecules, the heterotrimer laminin-5 which constitutes the BM-anchoring filaments located in the BM-lamina lucida and is essential for keratinocyte-BM-adhesion,[34] appeared in a spotty fashion at day 7 (Fig. 7A). At day 14, the dots were uniformly distributed with preference to the basal pole of the basal layer of keratinocytes (Fig. 7B). Interestingly, this preference found in vitro reflects the site of keratinocyte adhesion to the BM under in vivo conditions.[35] By tendency, this subepithelial preference at the basal pole at the later time point could also be noted for the other assessed BM-molecules, laminin-1/10 (Fig. 7D) and collagen type-IV (Fig. 7F). In analogy to laminin-5, the protein distribution of the latter-mentioned BM-constituents at day 14 considerably parallels that in vivo, while epithelia at 7 days exhibited a more intraepithelial distribution for laminin-1/10 (Fig. 7C), and an incomplete dotted sub-basal expression for collagen type-IV (Fig. 7E). As indicated by the insets of Figure 7, control epithelia at both observation periods showed only a sparse expression in the case of laminin-5 (inlays to Fig. 7A and 7B),

and laminin-1/10 (insets to Fig. 7C and 7D), respectively, while collagen type-IV was nearly absent (insets to Fig. 7E and 7F). With emphasis on the studied BM molecules, a very crucial finding is the default of the controls to exhibit their presence in an in vivo-like manner, that is, at sub-basal cell sites.

This adds to the body of evidence that the epithelial equivalents of the co-cultures resemble the in vivo phenotype of a gingival epithelium more closely, when compared to controls. Moreover, as already adumbrated by the gene expression studies and the protein orientation of the differentiation markers and DP as well, the patterns found for the ECM/BM molecules additionally prove that the fibroblast-harboring micropillar interfaces are the key component for the observed molecular in trans-regulation of the epithelial biomarkers.

3. Conclusions

An important implication of our study is that establishment and growth of GCTFs in their defined traction-force-sensing
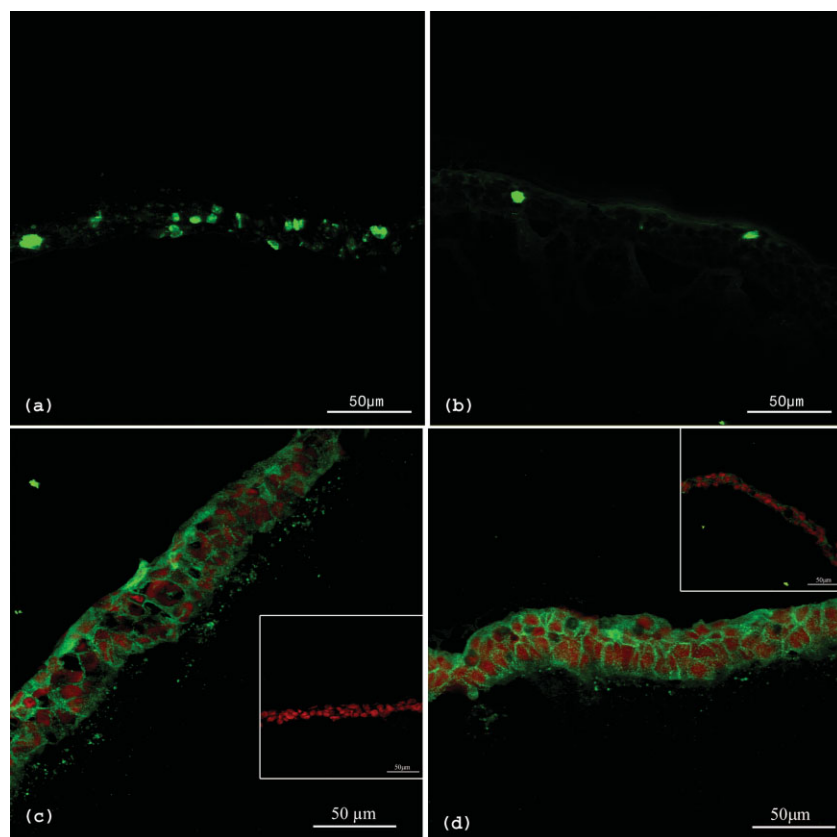
FULL PAPER

Figure 6. Indirect immunofluorescence illustrates the *Ki*-67 proliferation marker and the desmoplakin (DP) epithelial integrity marker in co-cultured epithelial equivalents generated on micropillar interfaces after 7 and 14 days, and their matched controls. The *Ki*-67 fluorescence indicates less-proliferative cells at day 14 (B) in comparison with signals after 7 days (A). DP is clearly detectable in the IHGK co-cultures at both time points (C, day 7) and, (D, day 14), but not in the controls at day 7 (C, inset), and only scattered at day 14 (D, inset). The red propidium iodide (PI) counterstain demarcates the cell nuclei. The scale bars correspond to 50 μm.

that the biological read-out does not only provide tissue-immanent new insights, but also allows for implications on a tissue in trans. In the case of an epithelium-underlying CT this in trans read-out addresses the epithelium, demonstrated here for the first-time. In the case of other periodontal CTs, such as the PDL, the in trans read-out would address the alveolar bone, since the PDL facilitates alveolar-bone anchorage of the tooth.[37] Hereby, the biomechanical and biological extracellular conditions that efficiently contribute to periodontal wound or tissue regeneration can be identified. In future, the knowledge of the biological consequences of targeted variation of predefined microenvironmental parameters assigned to biofunctionalization or biomechanics can be used for the optimization of existing cell-culture substrates. This in turn will lead from biocompatible to biomimetic materials or even to the creation of new materials applicable for proper tissue morphogenesis in regenerative dentistry and medicine.

4. Experimental

Pillar Fabrication and Biofunctionalization: - Molds with holes of defined height and diameter were created to achieve a homogeneous, thick layer of photoreactive polymer, which defines the structural height on a solid silicon wafer. The epoxy-based SU-8 10 resin (Microresist Technologies, Germany) was spin-coated with a defined speed onto a clean silicon wafer under clean-room conditions. Then, the solvent was evaporated by a two-step baking process. The wafer was exposed to UV light through a custom-made negative chromium mask. The photoinitiated ring-opening reaction was accomplished at 95 °C on a hotplate. Developing was performed in a developer containing propylene glycol monomethyl ether acetate (PGMEA) (mr-Dev.600, Microresist Technologies, Germany) for 1 min. For spin-coating, 2 ml of photoresist was spun on a silicon wafer ($\varnothing = 5.08$ cm) in a two-step process. To reach a 15 μm thickness, an SU-8 10 resist was spun on at 2000 rpm for 40 s. Next, softbaking of the wafer with 15 μm resist was done on a hotplate at 65 °C for 2 min followed by baking at 95 °C for 5 min. After cooling for 10 min to room temperature (RT), UV-exposure was performed on a mask aligner (MJB3, Karl Suess, Germany), equipped with a 400 W mercury lamp. The exposure time depended on the resist thickness and varied from 2.5 to 4 s. To complete cross-linking in the exposed areas, the wafer chips were heated up to 65 °C for 1 min, followed by heating up to 95 °C for 2 min and cooling to RT for ~10 min. To develop the structures, it was necessary to redissolve the unexposed parts in PGMEA for up to 1 min while shaking. The structure was blown dry with a stream of nitrogen. The silicon-based polymer PDMS (Dow Corning, Midland, Michigan, USA) was mixed vigorously with a short hydrosilane cross-linker in the ratio 10:1. To remove trapped air, the mixture was degassed for 30 min under vacuum at 7×10^{-2} mbar. The pillar arrays were then generated by pressing the molds upside down onto a drop of PDMS on a 24×24 mm coverslip, followed by curing for 6 h at 65 °C. After cooling

pillar-microenvironment is pivotal for epithelial tissue morphogenesis of IHGKs. To achieve cell adhesion on elastic PDMS pillar heads, we chose the ECM-component FN, which, amongst others, is also present in the gingival lamina propria.[36] In a previous study employing IHGKs, we demonstrated that FN immobilized on pillar heads is suitable to modulate keratinocyte differentiation in response to various pillar distances.[4] In the present study, we show for the first time that FN-coated pillar arrays of 9 μm distance and defined biomechanic properties allow for adhesion and growth of mesenchymal GCTFs. This finding may give a hint that also cells of other periodontal tissues which are descendents of the mesenchyme, such as osteoblasts of the alveolar bone and fibroblasts of the periodontal ligament (PDL) may be successfully established under these extracellular conditions. Thus, the chosen microenvironment can be prospectively used as a basis to study CT cell adhesion, growth, and gene expression and synthesis of cell-specific biomolecules by varying predefined microenvironmental parameters attributing to elasticity and/or ECM cell adhesion ligands. With respect to CT, this kind of variation study has the advantage
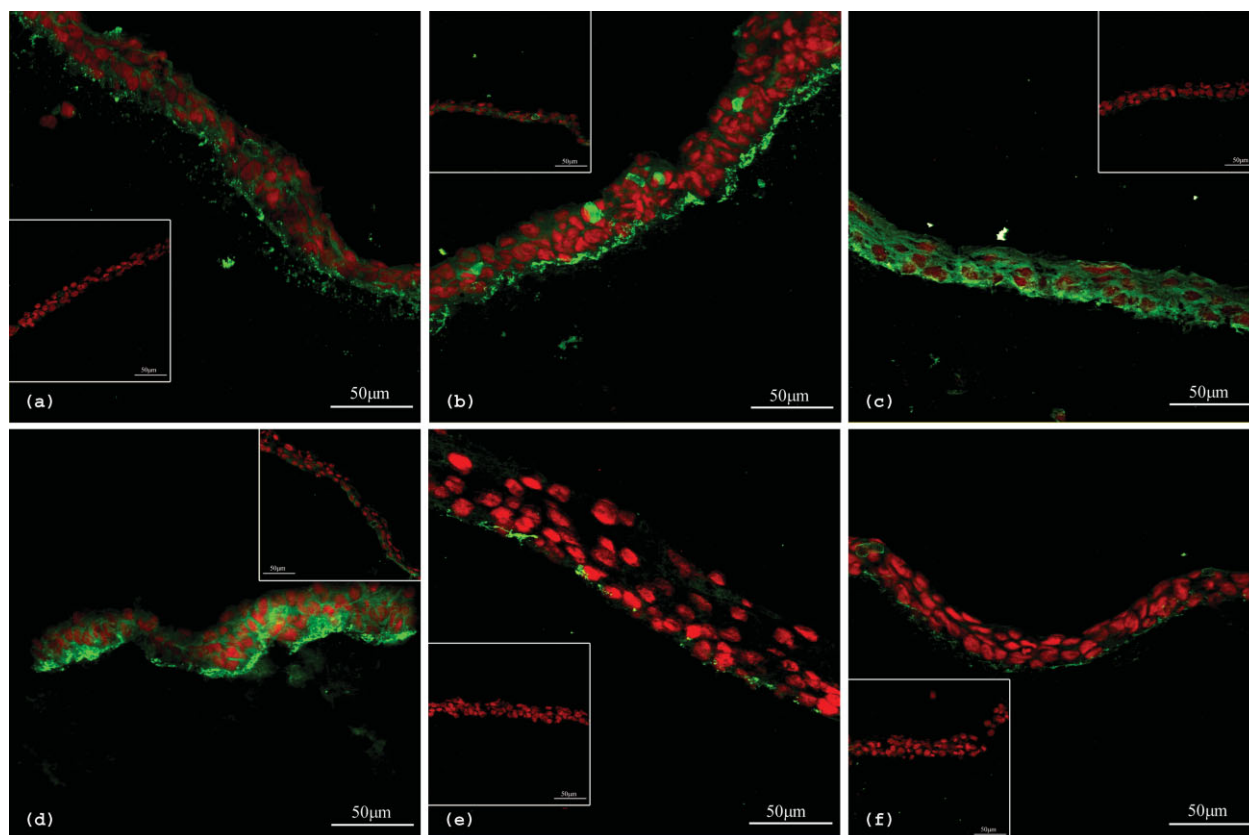
Figure 7. Indirect immunofluorescence illustrates the BM-constituting ECM molecules including laminin-5, laminin-1/10, and collagen type-IV in co-cultured epithelial equivalents generated on micropillar interfaces after 7 and 14 days, and matched controls. Laminin-5 appeared in a spotty fashion at day 7 (A) while at day 14, the fluorescence signal was uniformly distributed with preference to the basal pole of the basal keratinocyte layer (B). This distribution at the later time point could also be noted for the other assessed BM molecules: laminin-1/10 (D) and collagen type-IV (F). At day 7, laminin-1/10 exhibited a more-intraepithelial distribution for (C), and an incomplete, dotted, sub-basal expression for collagen type-IV (E). The insets depict the controls and indicate only a sparse expression for laminin-1/10 and laminin-5 (A–D; insets), while collagen type-IV is almost absent (E, F; insets). The red propidium iodide (PI) counterstain demarcates the cell nuclei. The scale bars correspond to 50 μm.

to RT, the substrates were peeled with a razor blade and overlapping PDMS residues were removed under sterile conditions. Each pillar array presented a dimension of 8×8 mm with a cultivation surface area of 64 mm^2. For the GCTFs, previous experiments employing different pillar interspaces revealed that these conditions could be considered as optimal with respect to cell morphology – cell spreading and shape formation. Therefore, the pillars used in this study had a height of 15 μm, a diameter of 5 μm and an interspace of 9 μm.

For depositing FN only to the pillar tops, drops (100 μl) of an FN solution (1 mg ml^{-1}, Sigma-Aldrich GmbH, München, Germany) in phosphate buffered saline (PBS) were pipetted carefully to the surfaces and incubated for 10 min at 4 °C. Immediately after withdrawing the drop, the surface was rinsed with PBS and directly used for cultivating cells on the pillar arrays.

Cell Culture: Establishment and serial cultivation of IHGKs has been reviewed recently [16]. To avoid medium-derived induction of keratinocyte differentiation, the IHGKs were maintained in low-calcium keratinocyte growth medium (basal keratinocyte medium, KGM, with provided supplements, Promocell, Heidelberg, Germany), containing 50 μg ml^{-1} kanamycin (Roche Diagnostics, Mannheim, Germany). GCTFs were cultured in Dulbecco's Modified Eagle's medium (DMEM) (PAA, Pasching, Austria) containing 10% foetal calf serum (Seromed, Biochrom, Berlin, Germany) for routine cell culture.

Generation of Co-cultures (CCs): Gingival connective-tissue fibroblasts (GCTFs) calibrated to a cell number of 1×10^5 cells per ml were precultured on the FN-coated pillar surfaces for 24 h in FAD medium (Ham's F12/DMEM: mixing ratio 1:3, Biochrom, Berlin, Germany) including 5% foetal calf serum (FCS) and additionally containing cholera toxin (8.33 mg ml^{-1}), hydrocortisone (0.4 mg ml^{-1}), epidermal growth factor (EGF) (0.01 mg ml^{-1}), and insulin (5 mg ml^{-1}) (all additives: Promocell, Heidelberg, Germany). Thereafter, a collagen lattice with a thickness of about 1mm and an extension equal to the size of the pillar array (about 64 mm^2) was carefully placed on the pillar tops. The collagen lattice was generated from a collagen type-I solution (4 mg ml^{-1}) (Curacyte, Leipzig, Germany) containing FCS and Hanks buffered salt solution ($10 \times$), and the whole mixture was polymerized at 37 °C. Then, immortalized human gingival keratinocytes (IHGKs) were seeded on the collagen-lattice surface at a density of 1×10^5 cells per ml. For optimal reproducibility at the announced periods of one and two weeks, three CCs of GCTFs and IHGKs were maintained in FAD medium. For control, 3 pillar arrays devoid of GCTFs were covered with the collagen lattice, and the IHGKs were seeded and cultured on the lattice surface as described previously. For RNA isolation, the IHGKs were accordingly seeded on the porous membrane of the trans-well filter insert (Greiner Bio-one, Frickenhausen, Germany). In the case of the CCs, pillars harbouring GCTFs were placed on the bottom of the trans-well, thereby facilitating spatial

separation from the IHGKs. All of the cell-culture experiments were conducted under standard cell-culture conditions: 37 °C, 97% humidity and 5% CO_2.

Raster Electron Microscopy (REM): After the respective culture periods on the micropillar surfaces, GCTFs were fixed with 4% glutaraldehyde in PBS for 1 h and rinsed 3 times with PBS buffer. Then, the specimens were dehydrated by rinsing through graded ethanol/water mixtures (50%, 70%, 80%, 90% and 100%; each step for 10 min at RT). Thereafter, ethanol was slowly exchanged by liquid CO_2. Finally, the samples were dried using the critical point method [38] and then sputtered with an thin layer of gold, of approximately 10 nm thickness.

Indirect Immunofluorescence (IIF): For IIF, the IHGK-epithelial equivalents derived from CCs and controls were carefully removed from the pillar surface, embedded in TissueTek (Sakura, Zoeterwoude, Netherlands), and frozen in liquid-nitrogen vapour. Then, 10 µm of frozen sections of the CC and control specimens were mounted on adhesive slides (Histobond, Marienfeld, Germany), followed by fixation in ice-cold, 80% methanol and acetone (5 min each). Thereafter, the frozen sections were incubated overnight with the primary antibodies directed against keratin K1/10 (mouse monoclonal/mab, Acris, Hiddenhausen, Germany, working dilution (wd) = 1:50), involucrin (mab, Abcam, Cambridge, United Kingdom, wd = 1:200), filaggrin (mab, Biozol, Eching, Germany, wd = 1:100), laminin-5 (rabbit, polyclonal, Progen, Heidelberg, Germany wd = 1:50), laminin-1/10 (rabbit, polyclonal, Progen, Heidelberg, Germany, wd = 1:50), collagen type-IV (mab, Progen, Heidelberg, Germany, wd = 1:10), Desmoplakin (mab, Santa Cruz Biotechnology, Heidelberg, Germany, wd = 1:10) and *Ki*-67 (mab MIB-1, Dako Deutschland GmbH, Hamburg, Germany wd = 1:10). Then, the slides were washed in PBS three times (5 min each), followed by incubation with the secondary fluorochrome-conjugated antibody (for K1/10, laminin-5, collagen type-IV, Desmoplakin and *Ki*-67: Alexa FluorTM 488, MoBiTec Göttingen, Germany; IgG (H+L) goat anti-mouse, wd = 1:50 and for Involucrin and Filaggrin wd = 1:100; for Laminin-1/10: Alexa FluorTM 488, MoBiTec Göttingen, Germany; IgG (H+L) goat anti-rabbit, wd = 1:50) for 1 h at room temperature. To allow for total nuclei counterstaining, propidium iodide (Sigma, Deisenhofen, Germany; wd = 1:1000) was added to the secondary antibody. All of the antibodies were adjusted to their final wd in PBS containing 0.01% TWEEN 20 (Sigma, Munich, Germany) and 12% bovine serum albumin (BSA) (Serva, Heidelberg, Germany) (PBT). Finally, the frozen sections were embedded in a mounting medium (Biomeda; Foster City; CA; United States) and studied by confocal laser scanning microscopy (CLSM, Leica TCS/NT, Leica, Bensheim, Germany).

IIF of GCTFs Established on Micropillar Interfaces: IIF of GCTFs established on FN-biofunctionalized micropillar interfaces was performed according to the operation mode described for the epithelial equivalents. Mabs directed against human vimentin (Acris, Hiddenhausen, Germany) and collagen type-I (Biodesign International, Saco, Maine, United States) were adjusted to a final working dilution of 1:20 in PBT, and secondary fluorochrome-conjugated antibody (Alexa Fluor 488®, MoBiTec GmbH, Göttingen, Germany, wd = 1:50) was used. Generally, the specificity of the employed primary antibodies was proven by only incubating the secondary antibody, which yielded no fluorescence signal.

RNA-Isolation and Quantitative Real-Time-PCR Analysis (qPCR) of Epithelial Equivalents and GCTFs: For qPCR, the epithelial equivalents of the co-cultures and controls, and the pillar arrays with GCTFs were maintained in the above-mentioned trans-well system. After the respective culture periods, the total RNA was isolated selectively from both cell types using the RNeasy mini kit (Qiagen, Hilden, Germany) after a period of one and two weeks. The specimens-derived RNA concentration and integrity was determined by using an automated electrophoresis system (Experion™ BioRad, München, Germany). First-strand cDNA was synthesized from a 1 µg total RNA aliquot in the reaction mixture, containing random hexamer primer, by performing the RevertAid™ reverse transcription protocol

(Fermentas Inc., Hanover, MD, USA). The cDNA concentration was determined by fluorometry using a fluorescence dye (PicoGreen; Molecular Probes) and adjusted to 1 ng µl^{-1}. qPCR analysis was performed with the iCycler real-time PCR detection System (BioRad Laboratories, Philadelphia, PA, USA) according to the manufacturer's instructions. In the case of the IHGKs, commercially designed primer pairs were used (RT2 PCR Primer Set for Human KRT1, KRT10, Involucrin and Filaggrin, Superarray, Frederick, MD, USA). The standard temperature profile included initial denaturation for 15 min at 95 °C, followed by 40 cycles of denaturation at 94 °C for 40 s, annealing at 55 °C (primer-dependent) for 30 s, and extension at 72 °C for 40 s. qPCR analysis of the GCTFs was accomplished with self-designed primers (Beacon Designer 5.0 Software, BioRad Laboratories, Philadelphia, PA, USA), for collagen type-I (forward: 5′-CGGAGGAGAGTCAG-GAAGG-3′; reverse 5′-ACATCAAGACAAGAACGAGGTAG-3′) nd vimentin (forward: 5′-TTTTTCCAGCAAGTATCCAACC-3′, reverse: 5′-GTTTTCCAAAGATTTATTGAA-3′, Thermo Fisher Scientific, Germany). The relative expression levels of each mRNA were analyzed using a modification of the $\Delta\Delta C_T$ equation, which allows counting for differences in efficiencies ($E = 10^{-1/\text{slope}}$) between the PCR reactions [39]. The data were calculated using the Gene Expression Macro software provided with the iCycler. The data were normalized to the C_T of the glycerinaldehyd-3-phosphat-dehydrogenase (GAPDH) non-modulated housekeeping gene. The data presented in Figure 2 and 4 reflect the means ($n = 3, \pm$ SD) of three independent experiments.

Measurement of Traction Forces: Phase-contrast live-cell imaging was used to localize empty and GCTF-covered pillar tops. A regular spaced pillar representing the ideal non-deflected position served as a control pillar. The position of the center of the pillars was recorded over 18 h using a numerical aperture 20× objective for live-cell imaging (Delta-Vision Core®, Applied Precision, Issaquah, WA, USA). For the measurement, the micropillar deflection was determined using image-analysis software written in MATLAB 6.0 (Mathworks). After enhancing the contrast of the pictures the pillars were approximated to a Gaussian followed by a Gaussian smoothing to track the pillar's centre of intensity. The distance between the real (cells attached to pillar tops) and ideal (empty control pillar tops) position of the tops was determined. The pillar stiffness was calculated to be 0.07 N m^{-1} (pillar dimensions: diameter = 5 µm, height = 15 µm); the forces acting on the pillar could be determined by Equation (1) [29]

For technical reasons the error of the resolution of the traction forces was approximated to 5 nN. This limitation is due to the restricted resolution of the image-acquisition system in phase-contrast microscopy.

[1] J. L. Tan, J. Tien, D. M. Pirone, D. S. Gray, K. Bhadriraju, C. S. Chen, *Proc. Natl. Acad. Sci. USA* **2003**, *100*, 1484.

[2] C. A. Lemmon, N. J. Sniadecki, S. A. Ruiz, J. L. Tan, L. H. Romer, C. S. Chen, *Mech. Chem. Biosystems* **2005**, *2*, 1.

[3] O. du Roure, A. Saez, A. Buguin, R. H. Austin, P. Chavrier, P. Silberzan, B. Ladoux, *Proc. Natl. Acad. Sci. USA* **2005**, *102*, 2390.

[4] T. Steinberg, S. Schulz, J. P. Spatz, N. Grabe, E. Mussig, A. Kohl, G. Komposch, P. Tomakidi, *Nano Lett.* **2007**, *7*, 287.

[5] C. Mohrdieck, A. Wanner, W. Roos, A. Roth, E. Sackmann, J. P. Spatz, E. Arzt, *Chem. Phys. Chem.* **2005**, *6*, 1492.

[6] C. Barentin, Y. Sawada, J. P. Rieu, *Eur. Biophys. J.* **2006**, *35*, 328.

[7] R. Merkel, N. Kirchgessner, C. M. Cesa, B. Hoffmann, *Biophysical J.* **2007**, *93*, 3314.

[8] A. Katsumi, J. Milanini, W. B. Kiosses, M. A. del Pozo, R. Kaunas, S. Chien, K. M. Hahn, M. A. Schwartz, *J Cell Biol.* **2002**, *158*, 153.

[9] N. Wang, E. Ostuni, G. M. Whitesides, D. E. Ingber, *Cell Motility Cytoskeleton* **2002**, *52*, 97.

[10] J. D. Kubicek, S. Brelsford, P. Ahluwalia, P. R. Leduc, *Langmuir* **2004**, *20*, 11552.

[11] L. D. Landau, E. M. Lifshitz, *Theory of Elasticity*, Pergamon Press, Oxford **1986**.

[12] M. Dembo, Y. L. Wang, *Biophysical J.* **1999**, *76*, 2307.

[13] K. Boehnke, N. Mirancea, A. Pavesio, N. E. Fusenig, P. Boukamp, H. J. Stark, *Eur. J. Cell Biol.* **2007**, *86*, 731.

[14] S. Werner, H. Smola, *Trends Cell Biol.* **2001**, *11*, 143.

[15] P. M. Bartold, L. J. Walsh, A. S. Narayanan, *Periodontol 2000*, **2000**, *24*, 28.

[16] G. Embery, R. J. Waddington, R. C. Hall, K. S. Last, *Periodontol 2000* **2000**, *24*, 193.

[17] R. Nischt, C. Schmidt, N. Mirancea, A. Baranowsky, S. Mokkapati, N. Smyth, E. C. Woenne, H. J. Stark, P. Boukamp, D. Breitkreutz, *J. Investigative Dermatology* **2007**, *127*, 545.

[18] H. J. Stark, M. Baur, D. Breitkreutz, N. Mirancea, N. E. Fusenig, *J. Investigative Dermatology* **1999**, *112*, 681.

[19] M. Roesch-Ely, T. Steinberg, F. X. Bosch, E. Mussig, N. Whitaker, T. Wiest, A. Kohl, G. Komposch, P. Tomakidi, *Differentiation* **2006**, *74*, 622.

[20] P. Tomakidi, N. E. Fusenig, A. Kohl, G. Komposch, *J. Periodontal Res.* **1997**, *32*, 388.

[21] P. Tomakidi, D. Breitkreutz, N. E. Fusenig, J. Zoller, A. Kohl, G. Komposch, *Cell Tissue Res.* **1998**, *292*, 355.

[22] D. B. Shannon, S. T. McKeown, F. T. Lundy, C. R. Irwin, *Wound Repair Regeneration* **2006**, *14*, 172.

[23] B. A. Harley, T. M. Freyman, M. Q. Wong, L. J. Gibson, *Biophysical J.* **2007**, *93*, 2911.

[24] W. Roos, J. Ulmer, S. Grater, T. Surrey, J. P. Spatz, *Nano Lett.* **2005**, *5*, 2630.

[25] T. Srisuwan, D. J. Tilkorn, J. L. Wilson, W. A. Morrison, H. M. Messer, E. W. Thompson, K. M. Abberton, *Periodontol 2000* **2006**, *41*, 88.

[26] J. M. Park, J. Y. Koak, J. H. Jang, C. H. Han, S. K. Kim, S. J. Heo, *Int. J. Oral Maxillofacial Implants* **2006**, *21*, 859.

[27] L. Scheideler, F. Rupp, H. P. Wendel, S. Sathe, J. Geis-Gerstorfer, *Dent Mater* **2007**, *23*, 469.

[28] M. Feghali-Assaly, M. H. Sawaf, G. Serres, N. Forest, J. P. Ouhayoun, *J. Periodontal Res.* **1994**, *29*, 185.

[29] A. Ganz, M. Lambert, A. Saez, P. Silberzan, A. Buguin, R. M. Mege, B. Ladoux, *Biol. Cell* **2006**, *98*, 721.

[30] P. Ye, C. C. Chapple, R. K. Kumar, N. Hunter, *J. Pathology* **2000**, *192*, 58.

[31] S. A. Smith, B. A. Dale, *J. Investigative Dermatology* **1986**, *86*, 168.

[32] E. Endl, C. Hollmann, J. Gerdes, *Methods Cell Biol.* **2001**, *63*, 399.

[33] V. Vasioukhin, E. Bowers, C. Bauer, L. Degenstein, E. Fuchs, *Nature Cell Biol.* **2001**, *3*, 1076.

[34] F. Spirito, S. Chavanas, C. Prost-Squarcioni, L. Pulkkinen, S. Fraitag, C. Bodemer, J. P. Ortonne, G. Meneguzzi, *J. Biol. Chem.* **2001**, *276*, 18828.

[35] K. M. Haas, A. Berndt, K. J. Stiller, P. Hyckel, H. Kosmehl, *J. Histochemistry Cytochemistry* **2001**, *49*, 1261.

[36] P. Walsh, L. Hakkinen, H. Pernu, M. Knuuttila, H. Larjava, *J. Periodontal Res.* **2007**, *42*, 144.

[37] A. Nanci, D. D. Bosshardt, *Periodontol 2000* **2006**, *40*, 11.

[38] W. Y. Yeong, C. K. Chua, K. F. Leong, M. Chandrasekaran, M. W. Lee, *J. Biomed. Mater. Res, Part B: Appl. Biomater.* **2007**, *82*, 260.

[39] K. J. Livak, T. D. Schmittgen, *Methods* **2001**, *25*, 402.